JOURNAL OF VIROLOGY, Nov. 2009, p. 11502–11513 Vol. 83, No. 22
0022-538X/09/$12.00 doi:10.1128/JVI.01318-09

Histone Deacetylases 1 and 2 Are Phosphorylated at Novel Sites during Varicella-Zoster Virus Infection▽

Matthew S. Walters,[1] Angela Erazo,[2,3] Paul R. Kinchington,[2] and Saul Silverstein[1]*

Department of Microbiology, College of Physicians and Surgeons, Columbia University, 701 W. 168th St., New York, New York 10032,[1] and Departments of Ophthalmology and of Molecular Microbiology and Genetics[2] and Graduate Program in Molecular Virology and Microbiology,[3] University of Pittsburgh, 203 Lothrop St., Pittsburgh, Pennsylvania 15213

Received 26 June 2009/Accepted 2 September 2009

ORF66p, a virion-associated varicella-zoster virus (VZV) protein, is a member of a conserved *Alphaherpesvirinae* kinase family with homology to herpes simplex virus U_S3 kinase. Expression of ORF66p in cells infected with VZV or an adenovirus expressing only ORF66p results in hyperphosphorylation of histone deacetylase 1 (HDAC1) and HDAC2. Mapping studies reveal that phosphorylation is at a unique conserved Ser residue in the C terminus of both HDACs. This modification requires an active kinase domain in ORF66p, as neither protein is phosphorylated in cells infected with VZV lacking kinase activity. However, hyperphosphorylation appears to occur indirectly, as within the context of in vitro kinase reactions, purified ORF66p phosphorylates a peptide derived from ORF62p, a known substrate, but does not phosphorylate HDAC. These results support a model where ORF66p is necessary but not sufficient to effect hyperphosphorylation of HDAC1 and HDAC2.

Because of their reliance on the host for efficient replication, viruses have evolved to hijack cellular machinery for this purpose. During this coevolution of virus and host, cellular antiviral defense mechanisms have developed that limit replication and subsequent spread of viruses (12, 48, 52). For large DNA viruses such as *Herpesviridae* that replicate within the nucleus, once the viral genome enters the nucleus, host proteins rapidly act to silence transcription from viral DNA and subsequently block or impair replication. For instance, efficient herpesvirus gene expression depends on inhibition of histone deacetylases (HDACs) (7, 20, 23, 40). HDACs are an ancient family of enzymes that have a major role in numerous biological processes (21). HDACs function by deacetylating lysine residues on histone tails, resulting in chromatin condensation and repression of gene expression (15). In conjunction with the antagonizing enzyme activity of histone acetyltransferases, HDACs and histone acetyltransferases provide a means for regulating, through chromatin alteration, transcriptional repression and activation, respectively (6, 16). To date, 11 different HDAC isoforms have been identified in mammalian genomes, and these are classified into four different families: class I (HDAC1, -2, -3, and -8), class II (HDAC4, -5, -6, -7, -9, and 10), and sirtuin class III and class IV (HDAC11) (21, 44). Because HDACs lack intrinsic DNA binding activity, they are recruited to target genes via direct association with transcription regulatory proteins, either individually or in large transcriptional repression complexes (53).

As a result of coevolution, viruses have evolved diverse strategies to overcome host defense mechanisms (12, 48, 52). Silencing of HDAC-containing complexes during herpes simplex virus type 1 (HSV-1) infection is blocked via multiple mechanisms. For instance, infected cell protein 0 (ICP0) of HSV-1 dislodges the LSD1/CoREST/REST complex from HDAC1 and HDAC2, disrupting the silencing effects of this repressor complex on viral promoters (17–19). In addition, HDAC1 and HDAC2 are phosphorylated in a U_S3 kinase-dependent manner (40), whereas phosphorylation of CoREST requires both U_S3 and U_L13 kinases (17). Following these events, a portion of LSD1, CoREST, REST, HDAC1, and HDAC2 translocates to the cytoplasm in an ICP0-independent manner (17, 18). The outcome of these processes allows for efficient viral gene expression and robust replication. Further analysis of these functions by autonomous expression studies demonstrates that both ICP0 and the U_S3 protein kinases (U_S3 and $U_S3.5$) independently block histone deacetylation to enable gene expression by distinct mechanisms (39).

Like HSV-1, varicella-zoster virus (VZV), the causative agent of varicella and zoster, is characterized as a human alphaherpesvirus (1). VZV encodes orthologs of both ICP0 and U_S3 kinase, termed ORF61p and ORF66p, respectively (34, 47). Like ICP0, ORF61p is a transcriptional activator and it enhances infectivity of viral DNA and targets ND10 components (29, 34, 35). In addition, a recent study suggests that ORF61p may have a role in inhibiting HDAC activity, further confirming the orthologous nature of these proteins (51). Although these proteins have similar functions, evidence suggests that they use distinct mechanisms to effect these changes to the host (29).

VZV ORF66p is a serine/threonine protein kinase highly homologous to the U_S3 family of protein kinases found only in alphaherpesviruses (32, 47). To date, the only well-characterized target of ORF66p is ORF62p, the major transcriptional regulatory protein of VZV. ORF66p directly phosphorylates ORF62p and modulates its cellular distribution during viral infection (9, 26–28). Based on their homology, it is suspected that ORF66p and U_S3 phosphorylate similar viral and cellular

* Corresponding author. Mailing address: Department of Microbiology, College of Physicians and Surgeons, Columbia University, 701 W. 168th St., New York, NY 10032. Phone: (212) 305-8149. Fax: (212) 305-5106. E-mail: sjs6@columbia.edu.

▽ Published ahead of print on 9 September 2009.

targets, although there are few data to substantiate this hypothesis. Both are known to share some functions, including the ability to block apoptosis of infected cells in a cell-type-dependent manner (36, 37, 42). At present, it is unknown if ORF66p phosphorylates HDAC1 and/or HDAC2 or if it has any role in blocking histone deacetylation to enhance VZV replication.

In this report, we demonstrate that HDAC1 and HDAC2 are hyperphosphorylated during VZV infection in an ORF66p-dependent manner. Autonomous expression of ORF66p is sufficient to induce hyperphosphorylation of these proteins, and its kinase activity is essential for this event. In addition, we also show that ORF66p targets phosphorylation of HDAC1 and HDAC2 at a conserved phosphorylation site within the C termini of both proteins, and this occurs by an indirect mechanism. In addition, pretreatment of cells with sodium butyrate, an HDAC inhibitor, partially complements growth of an ORF66p kinase-deficient VZV. These data suggest that ORF66p kinase activity targets HDAC1 and HDAC2 to inhibit viral genome silencing and allow efficient viral replication. Thus, we have identified HDAC1 and HDAC2 as new indirect targets of VZV ORF66p protein kinase and postulate that ORF66p functions in a way analogous to HSV-1 U_S3 kinases to inhibit HDAC activity and promote efficient VZV replication.

MATERIALS AND METHODS

Mammalian cells. Human melanoma cells (MeWo) and 293A cells were maintained as described previously (50). Twenty-four hours prior to transformation or infection, cells were seeded into culture dishes. For indirect immunofluorescence experiments, glass coverslips were added before seeding.

Transformation/transfection of cells. 293A cells were transformed with DNA using Fugene HD (Roche, Indianapolis, IN). SF9 cells were transfected with Cellfectin reagent (Invitrogen, Carlsbad, CA).

Viruses. (i) VZV. VZV-WT, VZV-ORF66KD, and VZV-ORF47Stop were described previously (10, 11, 22). Cell-associated and cell-free virus stocks were prepared and titrated as previously described (29).

(ii) Adenoviruses. The adenoviruses AdEmpty, AdTetOff, AdORF66WT, and AdORF66KD were described previously (10, 50).

(iii) Baculoviruses. Hemagglutinin (HA)-tagged ORF66 wild-type (ORF66WT) or kinase-deficient mutant (ORF66KD) genes used to create baculoviruses were detailed previously. The sequences encoding these proteins were excised using BstZ17I and PstI from pGK2-HA66 or pGK2-HA66KD, respectively (9). HA66KD contains D206E and K208R changes in the catalytic loop domain (27). Each was cloned into pAcGHLT-A (Clontech Laboratories, Inc., Mountain View, CA) cleaved with SmaI and PstI so as to be in frame with the six-His tag and glutathione *S*-transferase (GST). Baculoviruses expressing GST-tagged ORF66WT and ORF66KD were derived using the BaculoGold system (BD Pharmingen, San Diego, CA), by cotransformation of the plasmids with BaculoGold DNA using Cellfectin reagent (Invitrogen, Carlsbad, CA) into SF9 cells. SF9 cells were maintained as described previously (9). Virus from the primary supernatant was subsequently amplified and tested for expression alongside a control baculovirus expressing GST using HA- or GST-specific antibodies by Western blot analyses.

Plasmid construction. (i) Enhanced green fluorescent protein (EGFP) plasmids. pEGFP-C1 was purchased from Clontech Laboratories, Inc. (Mountain View, CA). pEGFP-ORF66 was previously described (10).

(ii) FLAG-HDAC1 plasmids. Wild-type human HDAC1 was amplified from pcDNA-HDAC1 (a gift from Daniel Wolf, Columbia University, New York, NY) using specific forward (F) and reverse (R) primers (F, 5′-GGGAATTCATGGCACAGACGCAGGGCACC-3′, and R, 5′-GAGCTCATAAAGACTACACGCCATGGG-3′) containing EcoRI and XhoI sites, respectively, and Vent DNA polymerase (New England Biolabs, Inc., Beverly, MA). The PCR product was subsequently cloned into EcoRI/XhoI-digested pCMV-Tag2B (Stratagene, La Jolla, CA) to yield pFLAG-HDAC1. By using a QuikChange II site-directed mutagenesis kit (Stratagene, La Jolla, CA), specific primers, and pFLAG-HDAC1 as template, the following mutants were generated: pFLAG-S393A (F, 5′-CCATCCCTGAGGAGGCTGGCGATGAGGACGAAGACGACC-3′, and R, 5′-GGTCGTCTTCGTCCTCATCGCCAGCCTCCTCAGGGATGG-3′), pFLAG-S406A (F, 5′-GACGACCCTGACAAGCGCATCGCGATCTGCTCCTCTGACAAACG-3′, and R, 5′-CGTTTGTCAGAGGAGCAGATCGCGATGCGCTTGTCAGGGTCGTC-3′), pFLAG-S410A (F, 5′-GCGCATCTCGATCTGCTCCGCTGACAAACGAATTGCCTGTGAG-3′, and R, 5′-CTCACAGGCAATTCGTTTGTCAGCGGAGCAGATCGAGATGCGC-3′), pFLAG-S421A (F, 5′-GCCTGTGAGGAAGAGTTCGCCGATTCTGAAGAGGAGGGAG-3′, and R, 5′-CTCCCTCCTCTTCAGAATCGGCGAACTCTTCCTCACAGGC-3′), and pFLAG-S423A (F, 5′-GAGGAAGAGTTCTCCGATGCTGAAGAGGAGGGAGAGGGGGG-3′, and R, 5′-CCCCCCTCTCCCTCCTCTTCAGCATCGGAGAACTCTTCCTC-3′). All primers used were manufactured by Operon Biotechnologies (Huntsville, AL), and all vector inserts were verified by DNA sequencing.

(iii) HDAC2 plasmids. Wild-type mouse HDAC2 cDNA (a gift from Ed Seto, University of South Florida, Tampa, FL) was cloned in frame into EcoRI-digested pCMV-Tag2B (Stratagene, La Jolla, CA) to yield pFLAG-mHDAC2. mHDAC2 is more than 99% identical to human HDAC2, with only two amino acid differences at positions 478 (Pro in mouse and Thr in human) and 480 (Ala in mouse and Thr in human). By using a QuikChange II site-directed mutagenesis kit (Stratagene, La Jolla, CA), specific primers (F, 5′-GTGAGAAAACAGACACCAAAGGAACCAAGTCAGAACAACTC-3′, and R, 5′-GAGTTGTTCTGACTTGGTTCCTTTGGTGTCTGTTTTCTCAC-3′), and pFLAG-mHDAC2 as template, amino acids 478 and 480 were altered to the human sequence to generate a plasmid (pFLAG-HDAC2) that expressed human HDAC2. The following mutants were generated using a QuikChange II site-directed mutagenesis kit (Stratagene, La Jolla, CA), specific primers, and pFLAG-HDAC2 as template: pFLAG-S394A (F, 5′-GGATGCTGTTCATGAAGACGCTGGAGATGAGGATGGAGAAG-3′, and R, 5′-CTTCTCCATCCTCATCTCCAGCGTCTTCATGAACAGCATCC-3′), pFLAG-S407A (F, 5′-GAAGACCCGGACAAAAGAATTGCCATTCGAGCATCAGACAAACGG-3′, and R, 5′-CCGTTTGTCTGATGCTCGAATGGCAATTCTTTTGTCCGGGTCTTC-3′), pFLAG-S411A (F, 5′-GAATTTCCATTCGAGCAGCAGACAAACGGATAGCTTGC-3′, and R, 5′-GCAAGCTATCCGTTTGTCTGCTGCTCGAATGGAAATTC-3′), pFLAG-S422A (F, 5′-GCGATGAAGAGTTTGCAGATTCTGAGGATGAAGGTG-3′, and R, 5′-CACCTTCATCCTCAGAATCTGCAAACTCTTCATCGC-3′), and pFLAG-S424A (F, 5′-GATGAAGAGTTTTCAGATGCTGAGGATGAAGGTGAAGGAG-3′, and R, 5′-CTCCTTCACCTTCATCCTCAGCATCTGAAAACTCTTCATC-3′). All primers used were manufactured by Operon Biotechnologies (Huntsville, AL), and all vector inserts were verified by DNA sequencing.

(iv) MBP plasmids. Plasmids expressing maltose binding protein (MBP) and MBP-IE62 fusion proteins containing IE62 residues 571 to 733 were described previously (9). MBPs containing wild-type murine HDAC2 and a mutant form of protein containing five Ala substitutions at Ser 394, 407, 411, 422, and 424 were expressed from plasmid DNAs derived from murine HDAC2 cDNAs (gifts from Ed Seto, University of South Florida, Tampa, FL) in frame with MBP in pMalC2 (New England Biolabs, Inc., Beverly, MA).

Dephosphorylation assay. Mock-infected or wild-type VZV-infected MeWo cells were harvested at 72 hours postinfection (hpi), washed twice with cold phosphate-buffered saline, scraped from tissue culture dishes, suspended in radioimmunoprecipitation lysis buffer (RIPA) (50 mM Tris HCl, pH 8.0, 150 mM NaCl, 0.5% NP-40) plus EDTA-free Complete protease inhibitor cocktail (Roche, Mannheim, Germany), and incubated on ice for 30 min. Lysates were clarified by centrifugation at 22,500 × *g* for 10 min in a Tomy MX-160 high-speed refrigerated microcentrifuge. Total protein concentration was measured using a Bio-Rad protein assay kit (Bio-Rad, Hercules, CA) (4). Thirty micrograms of total lysate was incubated at 37°C for 30 min with 20 units of calf intestinal alkaline phosphatase (CIAP; New England Biolabs, Inc., Beverly, MA) in dephosphorylation buffer provided by the manufacturer. Additional protease inhibitors (EDTA-free Complete protease inhibitor cocktail [Roche, Mannheim, Germany]) were added to the reaction mixture at a final concentration of 1×. The reactions were stopped by addition of 5× sodium dodecyl sulfate (SDS) sample buffer (250 mM Tris HCl, pH 6.8, 500 mM dithiothreitol, 10% SDS, 0.5% bromophenol blue, 50% glycerol). For control experiments, CIAP was inactivated by being heated at 95°C for 5 min with 50 mM EDTA before being added to dephosphorylation reaction mixtures.

Indirect immunofluorescence microscopy. Cells grown on glass coverslips were processed for indirect immunofluorescence, and images were acquired as described previously (50).

SDS-PAGE and Western blotting. Infected and transformed cells were processed for SDS-polyacrylamide gel electrophoresis (PAGE) and Western blotting analysis as previously described (50) using modified RIPA buffer (50 mM Tris HCl, pH 8.0, 150 mM NaCl, 0.5% NP-40, 50 mM NaF) plus Complete

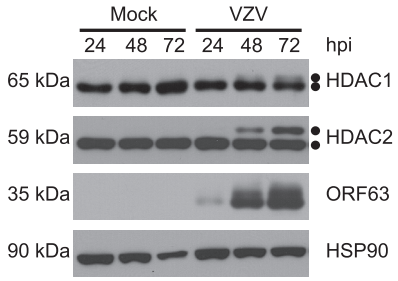

FIG. 1. Kinetic analysis of HDAC1 and HDAC2 forms during VZV infection. MeWo cells were mock infected or infected with cell-associated wild-type VZV at a multiplicity of infection of 0.025 and harvested 24, 48, and 72 hpi. At 72 hpi, all of the cells were infected as determined by phase microscopy and/or ORF66p-GFP expression. Equal amounts of total protein (20 μg) from each sample were analyzed by Western blotting using antisera specific for HDAC1, HDAC2, ORF63, and HSP90.

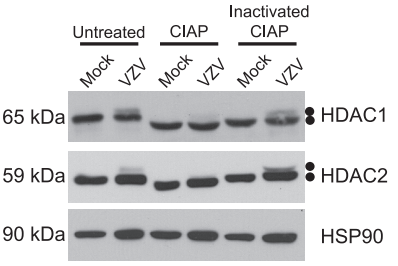

FIG. 2. Analysis of HDAC1 and HDAC2 in infected-cell extracts following incubation with CIAP. MeWo cells were mock infected or infected with cell-associated wild-type VZV at a multiplicity of infection of 0.025 and harvested at 72 hpi. At 72 hpi, all of the cells were infected as determined by phase microscopy and/or ORF66p-GFP expression. Lysates from mock- and VZV-infected cells were reacted with dephosphorylation buffer alone (untreated), CIAP, or inactivated CIAP as described in Materials and Methods. Equal amounts of total protein (20 μg) from each sample were analyzed by Western blotting using antisera specific for HDAC1, HDAC2, and HSP90.

protease inhibitor cocktail (Roche, Mannheim, Germany) and Halt phosphatase inhibitor cocktail (Pierce, Rockford, IL). Unless otherwise stated, all samples were electrophoretically separated on 7.5% polyacrylamide denaturing gels.

Protein purification. GST proteins were purified by solubilizing infected SF9 cells in RIPA buffer (20 mM Tris HCl, pH 8.5, 50 mM KCl, 1 mM EDTA, 1 mM dithiothreitol, 1% NP-40, and 0.5% deoxycholate) followed by sonication on ice after addition of EDTA-free mini-Complete protease inhibitor cocktail (Roche, Mannheim, Germany) and phosphatase inhibitors (50 mM sodium fluoride, 1 mM sodium orthovanadate, 10 mM β-glycerolphosphate, and 10 mM sodium pyrophosphate). Soluble fractions were combined with glutathione beads (Glutathione Uniflow resin; BD Pharmingen, San Diego, CA), mixed for 3 h or overnight, and washed extensively in 2 M KCl (pH 7.5), followed by RIPA buffer, and finally in kinase assay buffer (20 mM HEPES-KOH [pH 7.5], 50 mM KCl, 10 mM $MgCl_2$, and 5 μg/ml heparin). GST fusion proteins were eluted overnight at 4°C with glutathione elution buffer (BD Pharmingen, San Diego, CA) containing 0.1% Triton X-100. Protein levels were measured by the Bradford assay (4).

MBP substrates were purified as detailed previously (9) except that inductions were carried out in *Escherichia coli* BL21 cells at 30°C for 3 h.

In vitro kinase assay. Approximately 2 μg of GST, GST-ORF66p fusion protein, or casein kinase II (CKII) (New England Biolabs, Inc., Beverly, MA) was incubated with 2 μg of MBP or MBP fusion protein in a total volume of 70 μl in kinase assay buffer containing 5 μCi of [γ-^{32}P]ATP (6,000 Ci/mmol). Reactions were allowed to proceed for 25 min at 35°C and then stopped by addition of Laemmli SDS-PAGE sample buffer (30). Subsequently, proteins were separated on a 7% SDS-polyacrylamide gel and then transferred to a polyvinylidene difluoride membrane for autoradiography. Following exposure, membranes were subjected to Western blotting analysis using antisera specific to MBP or GST to ensure equivalent protein levels in each reaction mixture. Alternatively, following separation on a 7% SDS-polyacrylamide gel, proteins were stained with Coomassie brilliant blue (Invitrogen, Carlsbad, CA) staining solution to ensure equivalent protein levels in each reaction mixture before the gel was dried for autoradiography.

Drug treatment. Sodium butyrate ($C_4H_7O_2Na$) was purchased from EMD Biosciences (La Jolla, CA) and used as indicated in the figure legends.

Antibodies. All primary antibodies for Western blot analysis were used at dilutions between 1:1,000 and 1:5,000. Rabbit polyclonal antibody against ORF4, ORF61, ORF62, and ORF63 and mouse monoclonal antibody against gE were described previously (29, 31). Mouse monoclonal anti-FLAG M2 antibody, mouse monoclonal actin antibody, and rabbit polyclonal HDAC2 antibody were purchased from Sigma (St. Louis, MO). Mouse monoclonal antibody to HSP90 and rabbit polyclonal antibody to HDAC1 were purchased from Santa Cruz Biotechnology (Santa Cruz, CA). Mouse monoclonal antibody to GFP was purchased from Clontech Laboratories, Inc. (Mountain View, CA). Rabbit polyclonal antibody to MBP was purchased from New England Biolabs Inc. (Beverly, MA). Goat polyclonal antibody to GST was purchased from GE Healthcare (Piscataway, NJ). Alexa Fluor 546-conjugated rabbit anti-mouse antibody was purchased from Invitrogen (Carlsbad, CA). Goat anti-rabbit and anti-mouse antibodies conjugated to horseradish peroxidase for immunoblotting were purchased from Kirkegaard & Perry Laboratories (Gaithersburg, MD).

RESULTS

HDAC1 and HDAC2 are hyperphosphorylated in VZV-infected cells. As modulators of chromatin activity, HDACs are targeted during viral infection to block host gene silencing activities. It is known that HDAC activity is controlled by posttranslational modifications (8, 38, 49). To determine if HDAC1 and HDAC2 are modified during VZV infection, MeWo cells were either mock infected or infected with a wild-type VZV recombinant containing an amino-terminal fusion of EGFP to ORF66p. This virus allowed us to track the spread of infection in real time. The EGFP tag does not hinder viral replication or ORF66p activity (10). At 24, 48, and 72 hpi, cells were harvested and the electrophoretic mobilities of HDAC1 and HDAC2 were examined by Western blotting (Fig. 1). Staining for ORF63p and HSP90 was carried out as indicators of viral spread and a loading control, respectively. For HDAC1, two closely migrating protein species of approximately 66 kDa and 68 kDa were detected, with the 68-kDa species seen only in VZV-infected cells after 48 hpi, and it continued to accumulate as infection spread. Its abundance correlated with increased accumulation of ORF63p. Similarly to HDAC1, two HDAC2 species of approximately 59 kDa and 62 kDa were detected, again with the larger species present only in VZV-infected cells. The kinetics of accumulation of high-molecular-weight species of HDAC1 and HDAC2 were identical. The occurrence of novel, slowly migrating HDAC1 and HDAC2 species during VZV infection suggested that they were post-translationally modified in response to viral infection.

To determine if the altered species of HDAC1 and HDAC2 resulted from phosphorylation, mock-infected and wild-type VZV-infected cell lysates (harvested 72 hpi) were either untreated or treated with CIAP or inactivated CIAP. Following treatment, cell lysates were subjected to Western blot analysis to examine changes in protein mobility (Fig. 2). HSP90 was also analyzed to demonstrate equal loading of protein and as an indicator of any nonspecific protease activity associated with CIAP. In lysates from mock-infected cells, HDAC1 migrated as a single species. As expected, the mobility of HDAC1 from lysates treated with inactivated CIAP was similar to that of untreated lysates, suggesting that CIAP was completely inac-

tivated. After treatment with CIAP, HDAC1 migrated more rapidly, demonstrating that it was phosphorylated by cellular kinases in uninfected cells, as previously described (38). As expected, when lysates from VZV-infected cells were examined, HDAC1 migrated as two distinct species. Treatment of VZV-infected cell lysates with CIAP resulted in loss of most of the slower-migrating species of HDAC1 and appearance of a single, more rapidly migrating form that is indistinguishable from that present in CIAP-treated mock-infected cell lysates. Inactivated CIAP had no effect on the mobility of either form of HDAC1 from VZV-infected cell lysates. These data demonstrate that VZV-induced modification of HDAC1 is sensitive to phosphatase treatment and therefore a result of virus-induced hyperphosphorylation. Analysis of HDAC2 from these same reactions yielded results identical to those observed for HDAC1, i.e., there is a basal level of HDAC2 phosphorylation in uninfected cells (consistent with previous studies [49]) and that CIAP treatment results in loss of the slower-migrating, VZV-induced form of HDAC2. Thus, during VZV infection, a fraction of both HDAC1 and HDAC2 is hyperphosphorylated.

ORF66 kinase activity is essential for VZV-induced HDAC1 and HDAC2 phosphorylation. VZV encodes two serine/threonine (Ser/Thr)-specific protein kinases encoded by open reading frames (ORFs) 47 and 66. ORF47p (a homolog of HSV-1 U_L13, Epstein-Barr virus BGLF4, and cytomegalovirus U_L97) is related to the CKII family of cellular proteins, targeting Ser/Thr residues preceded by acidic residues, and is conserved in all *Herpesvirinae* (25, 45, 47). ORF66p (an HSV-1 U_S3 homolog) is present only in *Alphaherpesvirinae* and is a basophilic kinase that phosphorylates Ser/Thr residues with a target motif similar to that recognized by protein kinase A (PKA) (9, 32, 47). Both kinases carry out important functions that are required for efficient viral replication in a cell-type-dependent manner (3, 11, 24). To ask if these viral kinases play a role in hyperphosphorylation of HDAC1 and HDAC2, we examined whether VZV mutants lacking either ORF47p or ORF66p kinase activity were capable of modifying these proteins. The ORF47 mutant virus (VZV-ORF47Stop) contains a premature stop codon at amino acid 166 that produces a truncated protein lacking kinase activity (22). The ORF66 mutant virus (VZV-ORF66KD) produces a full-length protein with two conservative mutations that result in abolishment of ORF66p kinase activity (11). MeWo cells were mock infected or infected with wild-type VZV (VZV-WT), VZV-ORF47Stop, or VZV-ORF66KD and harvested 24, 48, 72, and 96 hpi. Cell lysates were prepared, and HDAC1 and HDAC2 mobilities were examined (Fig. 3). As before, ORF63p and HSP90 were examined as surrogates for viral infection and protein loading, respectively. In cells infected with VZV-ORF47Stop, hyperphosphorylated HDAC1 and HDAC2 were detected 24 h later than in cells infected with wild-type virus. In addition, accumulation of hyperphosphorylated HDAC1 and HDAC2 never reached the levels present in cells infected with wild-type virus, despite equal infection rates at initiation. A reduced accumulation of hyperphosphorylated HDAC1 and HDAC2 in VZV-ORF47Stop-infected cells may reflect the slower replication kinetics of this virus as suggested by the kinetics of ORF63p accumulation. This may be because VZV-ORF47Stop is derived from the vaccine strain Oka, while VZV-WT and VZV-ORF66KD are derived from parental Oka. However, it is clear that modified forms of HDAC1 and HDAC2 accumulate during infection with VZV-ORF47Stop. Therefore, we conclude from these experiments that ORF47p kinase activity is not essential for hyperphosphorylation of HDAC1 and HDAC2 during VZV infection.

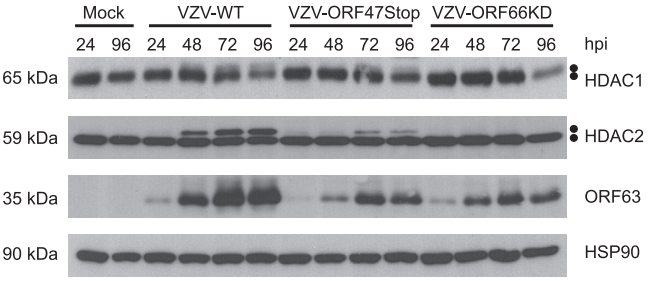

FIG. 3. Analysis of HDAC1 and HDAC2 hyperphosphorylation in cells infected with wild-type and kinase-deficient VZV. MeWo cells were mock infected or infected with cell-associated wild-type (VZV-WT), ORF47p kinase-deficient (VZV-ORF47Stop), or ORF66p kinase-deficient (VZV-ORF66KD) VZV at a multiplicity of infection of 0.025 and harvested 24, 48, 72, and 96 hpi. At 96 hpi, all of the cells were infected as determined by phase microscopy and/or ORF66p-GFP expression. Equal amounts of total protein (20 μg) from each sample were analyzed by Western blotting using antisera specific for HDAC1, HDAC2, ORF63, and HSP90.

In contrast to VZV-ORF47Stop, in cells infected with VZV-ORF66KD, HDAC1 and HDAC2 were not hyperphosphorylated during infection. Mutant virus replication was followed by ORF63p staining and was comparable to that observed with VZV-ORF47Stop. These data indicate that ORF66p kinase activity is required for hyperphosphorylation of HDAC1 and HDAC2 during VZV infection.

Replication-deficient wild-type (AdORF66WT) and kinase-deficient (AdORF66KD) adenoviruses expressing ORF66p tagged at their amino termini with EGFP under the control of a Tet-repressible promoter were used to ask if autonomous expression of ORF66p was sufficient to induce modification of HDAC1 and HDAC2 (10). Expression from these adenoviruses was dependent on coinfection with an adenovirus expressing the tetracycline tTa transactivator (AdTetOff) and the absence of doxycycline. MeWo cells were either mock infected or coinfected with AdEmpty (negative control), AdORF66WT, or AdORF66KD and AdTetOff. As a positive control, MeWo cells were infected with wild-type VZV. At 48 hpi, cells were harvested and lysed and the electrophoretic mobilities of HDAC1 and HDAC2 were examined (Fig. 4). EGFP and HSP90 were analyzed to confirm expression of ORF66p and protein loading for each sample. ORF66p levels were similar when expressed from VZV and when expressed from the adenovirus vectors. The apparent higher molecular weight of EGFP-ORF66 expressed from adenovirus backbones results from an HA tag within these proteins that is absent from wild-type VZV EGFP-tagged ORF66p. Analysis of HDAC1 and HDAC2 from cells infected with AdORF66WT revealed higher-molecular-weight species of HDAC1 and HDAC2 that were indistinguishable from those found in wild-type VZV-infected cells. These higher-molecular-weight species were absent from cells mock infected or infected with AdEmpty or AdORF66KD. These data demonstrate that autonomous ex-

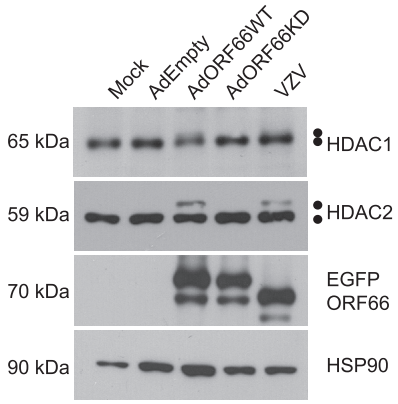

FIG. 4. Analysis of HDAC1 and HDAC2 in cells infected with adenoviruses expressing wild-type and kinase-deficient ORF66p. MeWo cells were mock infected or infected with AdEmpty, AdORF66WT, or AdORF66KD at a multiplicity of infection of 10 in conjunction with AdTetOff at a multiplicity of infection of 5. As a positive control, MeWo cells were infected with cell-associated wild-type VZV at a multiplicity of infection of 0.025. At 48 hpi, cells were harvested and equal amounts of total protein (20 μg) were analyzed by Western blotting using antisera specific for HDAC1, HDAC2, GFP, and HSP90.

pression of ORF66p induced hyperphosphorylation of HDAC1 and HDAC2 and that ORF66p kinase activity is essential for this event.

ORF66 hyperphosphorylation of HDAC1 and HDAC2 requires a conserved phosphorylation site within their C termini. HDAC1 and HDAC2 are the most highly conserved members of the HDAC superfamily, sharing 85% amino acid identity (14). Because of this high level of homology and their coexistence in the same protein complexes, these proteins play redundant and essential roles (33, 53). Cellular proteins posttranslationally modify both HDAC1 and HDAC2, and these modifications play a role in regulating their function (8, 38, 49). The best characterized of these posttranslational modifications is phosphorylation by cellular kinases within the highly conserved C termini of these proteins (38, 49). To further identify sites of ORF66p-mediated phosphorylation in HDAC1 and HDAC2, we used alanine insertion mutagenesis to block phosphorylation at potential target sites (Fig. 5A). To aid these studies, both HDAC1 and HDAC2 were cloned as amino-terminal FLAG fusion proteins to distinguish ectopically expressed from endogenous proteins. To validate this approach, 293A cells were cotransformed with plasmids expressing wild-type FLAG-HDAC1 (pFLAG-HDAC1) or FLAG-HDAC2 (pFLAG-HDAC2) and either EGFP (pEGFP) or EGFP amino-tagged wild-type ORF66p (pEGFP-ORF66). At 48 h post-transformation, cells were harvested and the electrophoretic mobilities of FLAG-HDAC1 and FLAG-HDAC2 were examined (Fig. 5B and C). All FLAG-HDAC proteins were identified using FLAG antibody, and membranes were probed for EGFP and HSP90 to confirm expression of ORF66p and to demonstrate equal protein loading. As expected, expression of FLAG-HDAC1 resulted in the appearance of only a single 70-kDa protein species. When FLAG-HDAC1 was coexpressed with wild-type ORF66p, an additional 72-kDa species was present, indicative of hyperphosphorylation of HDAC1. A similar result was observed for FLAG-HDAC2. When coexpressed with EGFP, FLAG-HDAC2 produced only a 64-kDa protein, whereas when ORF66p was present, an additional 66-kDa species was detected. These banding patterns were identical to those observed with endogenous HDACs in the absence and presence of ORF66p (Fig. 4). Cotransformation of tagged wild-type HDAC1 or HDAC2 with a kinase-dead mutant of ORF66p resulted in only a single species of each protein with a mobility identical to that seen in the absence of ORF66p (data not shown). In summary, these data demonstrate that FLAG-HDAC1 and FLAG-HDAC2 behave like endogenous proteins in that they are hyperphosphorylated when coexpressed with functional ORF66p.

HDAC1 and HDAC2 contain multiple conserved phosphorylation motifs that are recognized by several cellular kinases that predominantly target the region C terminal to residue 393 and 394 in the respective proteins (38, 49). Therefore, the dependence on ORF66p mediated hyperphosphorylation was examined by mutating known and potential Ser phosphorylation sites within FLAG-HDAC1 and FLAG-HDAC2. Individual Ser codons were changed to Ala in conserved casein kinase II (CKII), PKA, protein kinase C (PKC), and protein kinase G (PKG) sites in both genes (Fig. 5A) (Table 1). These sites were targeted because some were shown to be in vivo targets for phosphorylation of HDAC1 and HDAC2 and they are conserved in both proteins (38, 49). To evaluate the role of these sites in ORF66p hyperphosphorylation of HDAC1, 293A cells were cotransformed with pEGFP or pEGFP-ORF66p in conjunction with pFLAG-HDAC1 or a plasmid containing single-site mutations within HDAC1 (pFLAG-S393A, pFLAG-S406A, pFLAG-S410A, pFLAG-S421A, or pFLAG-S423A). After 48 h, cells were harvested and the electrophoretic mobility of FLAG-HDAC1 was examined (Fig. 5B). When cotransformed with EGFP, all FLAG-HDAC1 mutants behaved like the wild-type protein, producing only a 70-kDa species. When coexpressed with ORF66p, all mutants except S406A also produced a 72-kDa species that was indistinguishable from wild-type protein. Failure to detect the 72-kDa species from the S406A mutant suggested that ORF66p did not phosphorylate it and that S406 is a target for phosphorylation. This experiment was then repeated using pFLAG-HDAC2 or plasmids containing single Ser-to-Ala codon mutations within HDAC2 (pFLAG-S394A, pFLAG-S407A, pFLAG-S411A, pFLAG-S422A, or pFLAG-S424A) (Fig. 5C). As expected, all FLAG-HDAC2 mutants expressed only a single 64-kDa species when expressed with EGFP. However, when coexpressed with ORF66p, all mutant proteins except S407A also produced a 66-kDa species as wild-type FLAG-HDAC2 did. The failure of S407A to become hyperphosphorylated suggests that S407 is the target for ORF66p-mediated phosphorylation and this causes its differential migration on gels. These data reveal that a conserved phosphorylation site at S406 in HDAC1 and S407 in HDAC2 is a target for ORF66p-mediated in vivo phosphorylation. Notably, two basic residues at −2 and −3 precede these sites, consistent with the basophilic nature of the ORF66p target motif.

ORF66p-dependent phosphorylation of HDAC2 occurs by an indirect mechanism. Phosphorylation of HDAC1 and HDAC2 in ORF66p-expressing cells could be either a consequence of direct phosphorylation or a result of an indirect

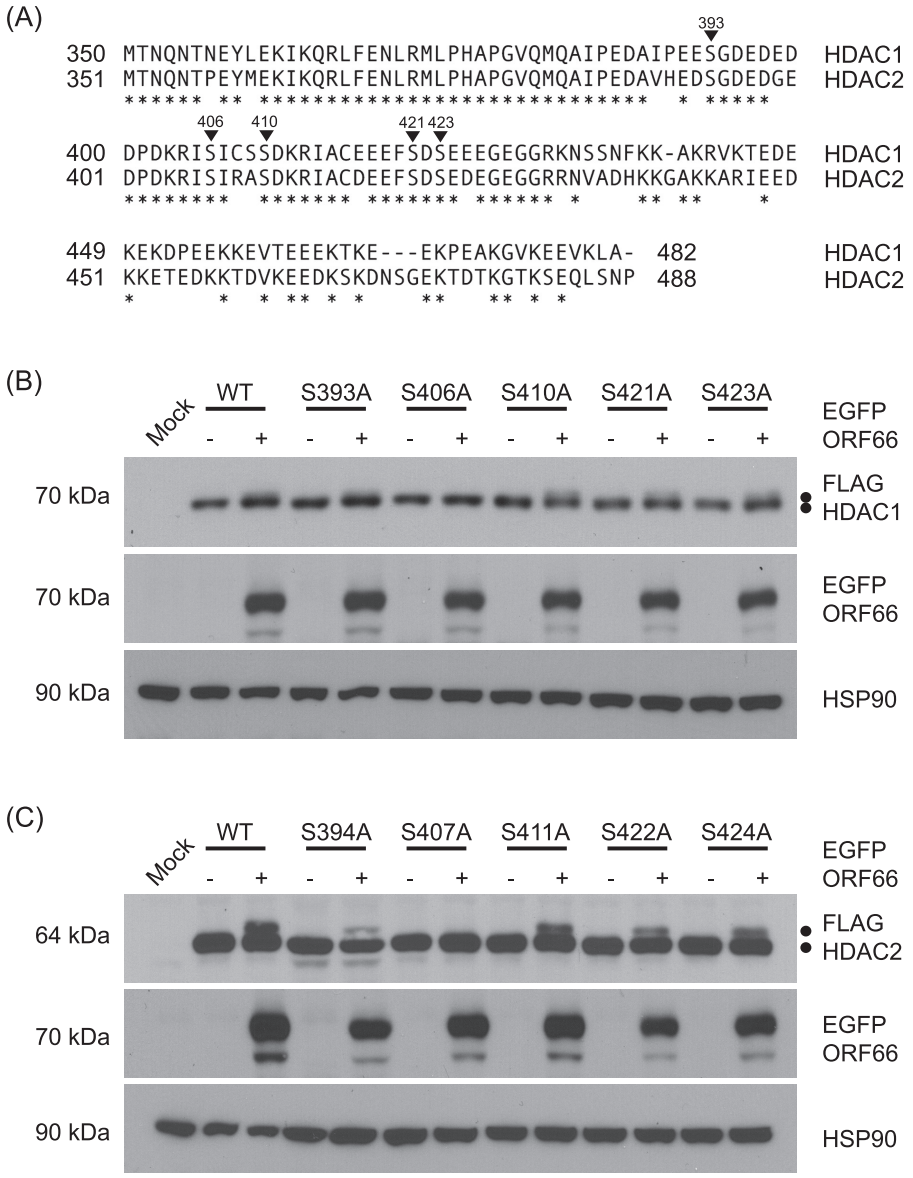

FIG. 5. Identification of Ser residues in HDAC1 and HDAC2 that are phosphorylated in response to ORF66p expression. (A) Amino acid sequence alignment of the C termini of HDAC1 and HDAC2. The amino acid sequences of HDAC1 and HDAC2 are aligned, and positions marked with asterisks identify identical amino acids. Inverted triangles indicate phosphorylation sites in both proteins. The numbers above each triangle correspond to residues in HDAC1. (B) To map the ORF66p target phosphorylation site(s) in HDAC1, 293A cells were mock transformed or cotransformed with 1 μg of either pFLAG-HDAC1, pFLAG-S393A, pFLAG-S406A, pFLAG-S410A, pFLAG-S421A, or pFLAG-S423A and 1 μg of pEGFP-C1 or pEGFP-ORF66. After 48 h, cells were harvested and equal amounts of total protein (20 μg) from each sample were analyzed by Western blotting using antisera specific for FLAG, GFP, and HSP90. (C) To map the ORF66p target phosphorylation site(s) in HDAC2, 293A cells were mock transformed or cotransformed with 1 μg of pFLAG-HDAC2, pFLAG-S394A, pFLAG-S407A, pFLAG-S411A, pFLAG-S422A, or pFLAG-S424A and 1 μg of pEGFP or pEGFP-ORF66. After 48 h, cells were harvested and equal amounts of total protein (20 μg) from each sample were analyzed by Western blotting using antisera specific for FLAG, GFP, and HSP90.

mechanism, such as ORF66p activation of a cellular kinase or pathway that leads to phosphorylation. To differentiate between these possibilities, we asked if ORF66p could directly phosphorylate HDAC1 and HDAC2. To test this, we developed an improved in vitro kinase assay, based on that previously described to characterize ORF66p phosphorylation of ORF62p (9). In this system, kinase substrates are fused with MBP and protein kinases are fused with GST; each is then purified by affinity binding. Wild-type murine HDAC2 and a mutant form of mouse HDAC2 (containing five Ala substitutions at Ser 394, 407, 411, 422, and 424) were cloned in frame with MBP to yield MBP-HDAC2WT and MBP-HDAC2MUT, respectively. Coexpression studies of wild-type mouse HDAC2 with ORF66p in 293A cells demonstrated that ORF66p phosphorylated the protein in a manner identical to that of human HDAC2 (data not shown). All MBP fusion proteins were expressed in *E. coli* and purified. GST-tagged wild-type (GST66WT) and kinase-deficient (GST66KD) ORF66p were expressed in SF9 cells using recombinant baculoviruses, and at 48 hpi GST-tagged proteins were purified (9). To determine if

TABLE 1. Potential VZV ORF66 kinase phosphorylation sites within HDAC1 and HDAC2

Kinase	Consensus	HDAC1 Ser residue	HDAC2 Ser residue
CKII	X(S/T)XX(D/E)	393 421 423	394 422 424
PKA	$RX_{1-2}(S/T)X$	406	407 411
PKC	X(S/T)X(R/X)	410	407 411
PKG	$(R/K)_{2-3}X(S/T)X$	406	407

ORF66p could directly phosphorylate HDAC2, equal amounts of GST or GST-ORF66p fusion proteins were incubated with equal amounts of MBP or MBP fusion proteins under optimal kinase conditions. After 25 min, target proteins were subjected to SDS-PAGE and analyzed for phosphorylation by autoradiography of dried gels. Coomassie blue staining and Western blot analyses were used to ensure that equivalent levels of GST and MBPs were in each reaction mixture (Fig. 6B). As expected, in reaction mixtures containing GST, MBP, or MBP fusion proteins alone (Fig. 6A, lanes 1, 4, 8, and 12), no specific phosphorylation was detected. However, when GST66WT was incubated alone, a phosphorylated protein of approximately 72 kDa that represented autophosphorylated ORF66p was detected (Fig. 6A, lane 2). The intensity of this band is greatly reduced for GST66KD (Fig. 6A, lane 3). This phosphorylation pattern is present in all reaction mixtures containing wild-type and kinase-deficient ORF66p GST fusions (Fig. 6A, lanes 2, 3, 6, 7, 10, 11, 14, and 15). Incubation of MBP with GST, GST66WT, or GST66KD had no effect on the phosphorylation patterns compared to incubation of these proteins alone (Fig. 6A, lanes 5 to 7). In contrast, an ORF62 peptide sequence that is a known direct target of ORF66p phosphorylation (9) was extensively phosphorylated. This 60-kDa protein, which is the expected size of the fusion protein, appears only after incubation with wild-type GST66 protein kinase (Fig. 6A, lane 10). The phosphorylation signal from MBP-62pep was drastically diminished upon incubation with GST66KD (Fig. 6A, lane 11). These data are consistent with previous studies and confirm that GST66 kinase directly phosphorylates MBP-62pep (9).

We next analyzed the nature of ORF66p phosphorylation of HDAC2. As expected, MBP-HDAC2WT was essentially not phosphorylated when incubated alone or with GST (Fig. 6A, lanes 12 and 13). Incubation of MBP-HDAC2WT protein with wild-type ORF66p (Fig. 6A, lane 14) did not result in a phosphorylation pattern indicative of ORF66p-directed in vivo phosphorylation. Indeed, there was no discernible difference between phosphorylation patterns of MBP-HDAC2WT protein incubated with GST66WT and of that incubated with GST66KD (Fig. 6A, lanes 14 and 15). This result suggested that HDAC2 is not a direct target of ORF66p. To confirm that HDAC2 can be phosphorylated in this assay, MBP-HDAC2WT was incubated with purified CKII which directly phosphorylates HDAC2 (49). As expected, HDAC2 was robustly phosphorylated by CKII (Fig. 6A, lane 16). However, the phosphorylation-resistant form of HDAC2 (MBP-HDAC2MUT) was not (Fig. 6A, lane 17). We conclude that HDAC2 is not a directly phosphorylated target of ORF66p

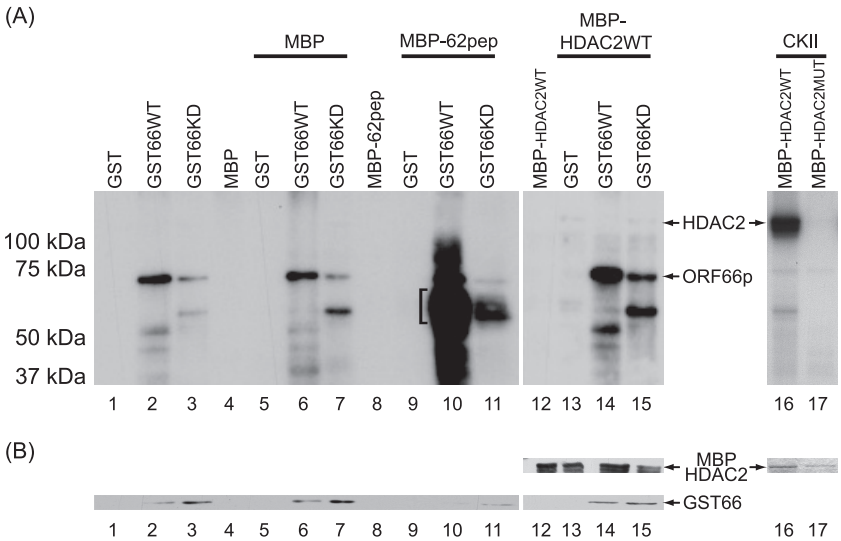

FIG. 6. In vitro analysis of ORF66p-dependent HDAC hyperphosphorylation. (A) Purified MBP substrate and GST kinase proteins were incubated in optimal kinase buffer, subsequently separated on 7% polyacrylamide denaturing gels, and then processed for autoradiography as described in Materials and Methods. Lanes 1 to 4 contain GST, GST66WT, GST66KD, and MBP incubated alone, respectively. Lanes 5 to 7 contain MBP incubated with GST, GST66WT, and GST66KD, respectively. The bracket in lane 10 identifies phosphorylated MBP-62pep. Lane 8 contains MBP-62pep incubated alone. Lanes 9 to 11 contain MBP-62pep incubated with GST, GST66WT, and GST66KD, respectively. Lane 12 contains MBP-HDAC2WT incubated alone. Lanes 13 to 15 contain MBP-HDAC2WT incubated with GST, GST66WT, and GST66KD, respectively. Lanes 16 and 17 contain CKII incubated with MBP-HDAC2WT and MBP-HDAC2MUT, respectively. (B) Equivalent levels of GST and MBP were detected in lanes 1 to 15 by Western blot analysis of the membranes following autoradiography. For lanes 16 and 17, Coomassie brilliant blue staining of the gel prior to drying and autoradiography was used to demonstrate equivalent levels of MBPs in each reaction mixture.

TABLE 2. Plaquing efficiency of wild-type and ORF66p kinase-deficient VZV in MeWo cells treated with sodium butyrate

Virus	Sodium butyrate treatment (1 mM)	Avg. no. of plaques	SD
VZV-WT	No	121.7	12.50
VZV-WT	Yes	122.0	14.32
VZV-ORF66KD	No	51.8	8.23
VZV-ORF66KD	Yes	78.7	5.92

kinase under conditions where ORF62pep, a known substrate, is directly phosphorylated.

HDAC activity affects plaquing efficiency, plaque size, and growth of a VZV ORF66p kinase-deficient mutant but not wild-type virus. Disrupting or inactivating ORF66p protein kinase affects VZV growth in a cell-type-dependent manner (11, 42, 43, 46). The functional roles of ORF66p that are necessary to direct efficient replication in these various cell types remain undefined. However, recent studies of the HSV-1 kinases homologous to ORF66p, U_S3 and $U_S3.5$, indicate that they mediate phosphorylation of HDAC1 and HDAC2 and boost viral gene expression (39–41). Treatment of cells with sodium butyrate, a potent inhibitor of class I and II HDACs, resulted in enhanced expression of viral or cellular genes, similar to what occurs in response to autonomous expression of either U_S3 or $U_S3.5$ kinase (40, 41). These findings suggest a role for U_S3 and $U_S3.5$ kinases in inhibiting gene-silencing functions of HDAC-containing complexes via phosphorylation of HDAC1 and HDAC2. Based on the similarity of ORF66p to U_S3 and $U_S3.5$ kinases and their conserved ability to phosphorylate HDAC1 and HDAC2, we posited that phosphorylation of HDAC1 and HDAC2 during VZV infection has a similar role. Therefore, we investigated the effect of blocking HDAC1 and HDAC2 activity on growth of VZV-ORF66KD.

Plaquing efficiency of wild-type VZV and VZV-ORF66KD in MeWo cells was first determined in cells treated with sodium butyrate to inhibit HDAC activity. Confluent monolayers of MeWo cells were untreated (mock) or treated with 1 mM sodium butyrate 6 h before infection. Following pretreatment, cells were infected with serial dilutions of cell-free virus and monolayers were maintained in medium with or without drug. Several days postinfection, monolayers were fixed and stained and plaques were counted (Table 2). Relative plaquing efficiency was calculated as number of plaques in the presence of drug/number of plaques in the absence of drug (Fig. 7A). Pretreatment of MeWo cells with sodium butyrate had no effect on plaquing efficiency of wild-type virus. In contrast, pretreatment of MeWo cells reproducibly increased plaquing efficiency of VZV-ORF66KD by 1.5-fold. While modest, this was determined to be significant [P of $t_{(pval)} = 0.0003$]. Thus, inhibiting HDAC activity increased the ability of VZV-ORF66KD to establish a productive infection.

Deletion of ORF66 or abolishment of its kinase activity results in a modest impairment of growth in several cell types (11, 42, 43, 46). We noted that the cytopathic effect and plaque size of wild-type virus were greater than those of VZV-ORF66KD. Therefore, we investigated what effect sodium butyrate treatment had on plaque size. MeWo cells on coverslips

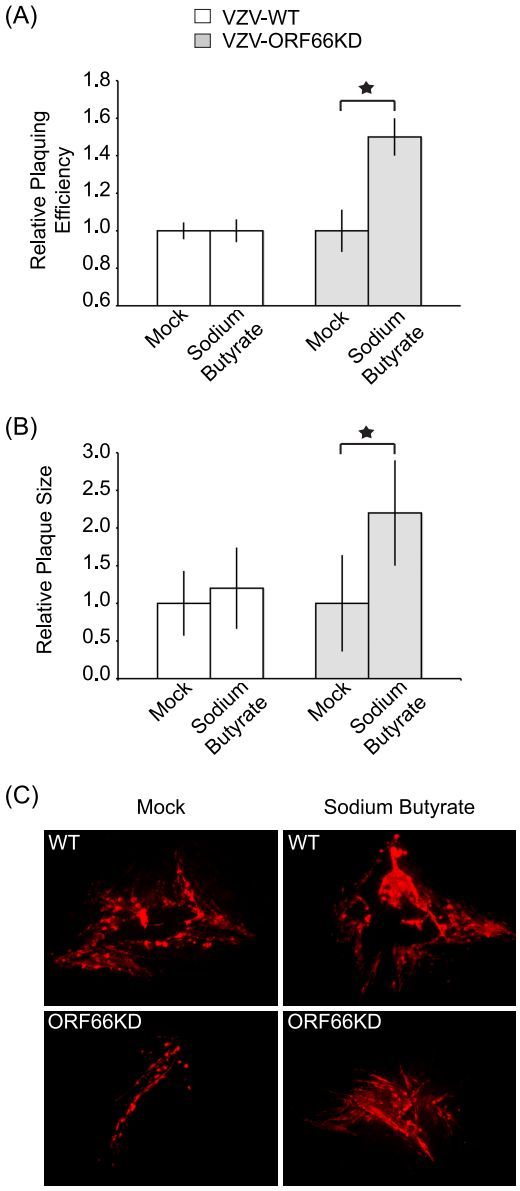

FIG. 7. Plaquing efficiency and plaque size of ORF66p kinase-deficient VZV in cells treated with sodium butyrate. (A) MeWo cells were mock treated or pretreated with 1 mM sodium butyrate for 6 h. Following treatment, cells were infected with serial dilutions of cell-free wild-type (VZV-WT) or ORF66p kinase-deficient (VZV-ORF66KD) VZV. Cells were maintained in medium in the absence or presence of 1 mM sodium butyrate. After 6 days, monolayers were fixed and stained and plaques were counted. Relative plaquing efficiency was calculated as described in the text. Each column represents the average from two independent experiments, and error bars indicate standard deviations. A star indicates a P value [$t_{(pval)} = 0.0003$] as determined by t test. (B) MeWo cells on coverslips were pretreated and infected as described above. Medium was replaced and fresh drug was added daily. Three days postinfection, cells were fixed, stained for gE, and observed by immunofluorescence microscopy. For each virus sample, images of 20 plaques were taken with a 10× objective and the size of each plaque was quantified using ImageJ software. The relative plaque size for each virus was calculated as described in the text. Results from a representative experiment are shown. Error bars indicate standard deviations. A star indicates a P value [$t_{(pval)} = 0.00008$] as determined by t test. (C) Representative images for the average relative plaque size for each virus in the absence (Mock) and presence of 1 mM sodium butyrate. Images were captured at 3 days postinfection using a 10× objective following fixation and staining for gE by immunofluorescence microscopy.

TABLE 3. Plaque size of wild-type and ORF66p kinase-deficient VZV in MeWo cells treated with sodium butyrate

Virus	Sodium butyrate treatment (1 mM)	Avg. plaque size (no. of pixels)	SD (no. of pixels)
VZV-WT	No	2.4×10^9	1.0×10^9
VZV-WT	Yes	3.0×10^9	1.3×10^9
VZV-ORF66KD	No	7.0×10^8	4.5×10^8
VZV-ORF66KD	Yes	1.5×10^9	4.9×10^8

were pretreated and infected as described above. Medium was replaced and fresh drug was added daily. Cells were fixed and stained for the viral glycoprotein gE. For each virus and condition, 20 plaques were imaged and the size of each plaque was quantified (Table 3). Relative plaque size for each virus was calculated as size of plaques in the presence of drug/size of plaques in the absence of drug (Fig. 7B). Representative images of plaques are shown in Fig. 7C. Analysis of wild-type VZV revealed that treatment of MeWo cells with sodium butyrate had only a marginal, nonsignificant effect {1.2-fold increase [$t_{(pval)} = 0.08$]} on plaque size. In contrast, as a result of treatment with sodium butyrate the plaque size of VZV-ORF66KD significantly increased {2.2-fold [$t_{(pval)} = 0.00008$]} (Fig. 7B). However, even in the presence of sodium butyrate, the average plaque size for VZV-ORF66KD was still smaller than that for wild-type virus, suggesting that inhibition of deacetylase activity only partially complemented the growth impairment of VZV deficient for ORF66p activity (Table 3). We conclude that inhibition of HDAC activity results in increased plaque size and spread of VZV-ORF66KD.

Because VZV is so highly cell associated and cell-free virus has very high particle-to-PFU ratios, in the range of 40,000 (5), we decided to study formation of infectious centers by both wild-type virus and VZV-ORF66KD in the absence and presence of sodium butyrate. MeWo cells were treated as described previously and infected with cell-free wild-type virus or VZV-ORF66KD. At various times postinfection, infectious centers were measured (Fig. 8A). Without sodium butyrate, the num-

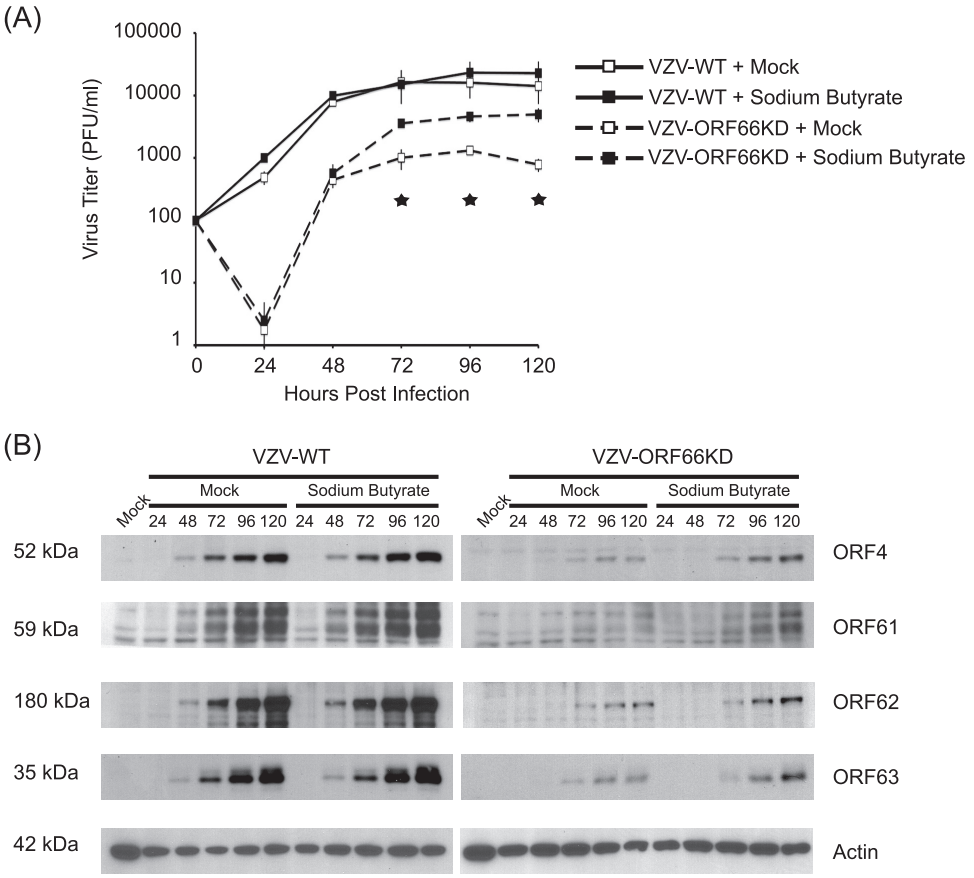

FIG. 8. Effect of inhibition of HDAC activity on growth and viral gene expression in cells infected with ORF66p kinase-deficient VZV. (A) MeWo cells were mock treated or pretreated with 1 mM sodium butyrate for 6 h. Following treatment, cells were infected with cell-free wild-type (VZV-WT) or ORF66p kinase-deficient (VZV-ORF66KD) VZV at a multiplicity of infection of 0.0001. Cells were maintained in medium with or without 1 mM sodium butyrate as indicated, and medium was replaced daily. At 24-h intervals postinfection, cell-associated virus titers were measured by titration on fresh monolayers of MeWo cells. Five days postinfection, monolayers were fixed and stained and plaques were counted to calculate the titers of infectious centers. Each datum point represents the average from two independent experiments, and the error bars indicate standard deviations. Stars identify *P* values [$t_{(pval)} < 0.006$] for VZV-ORF66KD at 72, 96, and 120 hpi, as determined by *t* test. (B) MeWo cells were pretreated as described previously and infected with cell-free wild-type (VZV-WT) or ORF66p kinase-deficient (VZV-ORF66KD) VZV at a multiplicity of infection of 0.0001. Postinfection, cells were maintained as described above. At the indicated time points postinfection, cells were harvested and equal amounts of total protein (20 μg) were analyzed by Western blotting using antisera specific for ORF4p, ORF61p, ORF62p, ORF63p, and actin.

ber of wild-type VZV infectious centers increased early in infection before reaching a plateau between 48 and 72 hpi. Thereafter, the titer remained constant. In contrast, the number of VZV-ORF66KD infectious centers dropped dramatically at 24 hpi, before increasing at 48 hpi. At 48 hpi, the titer of ORF66p kinase-deficient VZV was equivalent to that of wild-type VZV at 24 hpi, demonstrating a lag in spread compared to that of wild-type virus. After 72 hpi, infectious centers generated by VZV-ORF66KD reached a plateau and remained constant, but consistently with previous reports, the peak titer of ORF66 kinase-deficient VZV was around 10-fold lower than that for wild-type virus (11). In the presence of sodium butyrate, infectious centers generated by wild-type virus were virtually identical at all time points compared to those of untreated cells. Growth curve analysis of VZV-ORF66KD in cells treated with sodium butyrate demonstrated no difference in growth kinetics or formation of infectious centers up to 48 hpi compared to those of virus grown in the absence of drug. However, at 72 hpi there was a fourfold increase [$t_{(pval)} = 0.0005$] in infectious centers in cells grown with sodium butyrate over those in cells grown without drug. Moreover, sodium butyrate treatment allowed VZV-ORF66KD to reach a higher plateau than that of untreated cells, although it never reached the level of wild-type virus. Sodium butyrate was unable to fully complement the growth defect of VZV-ORF66KD. In summary, inhibiting HDAC activity increases growth and yield of VZV-ORF66KD.

We then examined the expression patterns of viral proteins at various time points to ask what role inhibition of HDAC activity had on increased growth and yield of VZV-ORF66KD. To address this question, cells from each time point of a growth curve were harvested and analyzed for accumulation of viral immediate-early gene products ORF4p, ORF61p, ORF62p, and ORF63p. Analysis of Western blots revealed that ORFs 4p, 61p, 62p, and 63p were detectable by 48 hpi following infection with cell-free virus and continued to accumulate as infection proceeded (Fig. 8B). There was no difference in accumulation of these proteins between cells that were mock treated and those that were treated with sodium butyrate for wild-type virus, consistent with the growth curve analysis.

For VZV-ORF66KD, viral proteins were detected at 72 hpi. While at this time there was no difference in accumulation of ORFs 4p, 62p, and 63p in cells treated with sodium butyrate or left untreated, it was apparent that at 96 and 120 hpi, the abundance of these proteins was increased in sodium butyrate-treated cells. The most significant difference was observed for ORF61p. ORF61p accumulation in mock-treated cells was barely detected at 120 hpi; however, in cells treated with sodium butyrate, it was easily detectable at 72 hpi and continued to accumulate as infection progressed. Thus, an increase in the abundance of ORF61p and its more rapid appearance in sodium butyrate-treated cells correlated with the increased yield of VZV-ORF66KD. In summary, we demonstrate that inhibition of HDAC activity enhances growth of ORF66p kinase-deficient VZV.

DISCUSSION

Once a herpesvirus genome enters the nucleus, host proteins rapidly act to silence transcription from viral DNA and subsequently block or impair replication. One example in which the host silences viral genomes is through the HDAC family of enzymatic proteins that deacetylate lysine residues on histone tails, resulting in chromatin condensation and subsequent repression of gene expression (15). Herpesviruses have evolved diverse mechanisms to block silencing of HDAC repressor complexes (17–19, 39, 40). One aspect of this strategy during HSV-1 infection involves phosphorylation of HDAC1 and HDAC2 via the HSV-1 Ser/Thr U_S3 kinases (39, 40). The outcome of phosphorylation allows for efficient viral gene expression and robust replication. Until this study, it was not known if VZV, another human alphaherpesvirus (1), possessed the capacity to subvert HDAC-mediated restriction.

The purpose of this report was to investigate if HDACs were modified during VZV infection and, if so, how this affected VZV replication. As a starting point, we infected MeWo cells with wild-type VZV and harvested samples over time to ask if any changes occurred in the electrophoretic mobilities of HDAC1 and HDAC2 (Fig. 1). As VZV infection progressed, novel, slower-migrating species of HDAC1 and HDAC2 appeared. In vitro dephosphorylation assays revealed that HDAC1 and HDAC2 are hyperphosphorylated during infection (Fig. 2). The HSV-1 U_S3 kinases are required for phosphorylation of HDAC1 and HDAC2 (39–41), and VZV encodes ORF66p, an ortholog of these proteins (36, 37, 42, 47). We demonstrate that a VZV mutant lacking ORF66p kinase activity is unable to induce hyperphosphorylation of HDAC1 and HDAC2 (Fig. 3). In addition, autonomous expression of ORF66p results in hyperphosphorylation of HDAC1 and HDAC2, and its kinase activity is essential for this event (Fig. 4). These data demonstrate that HDAC1 and HDAC2 are novel targets for ORF66p and highlight a conserved target substrate between ORF66p and its HSV-1 orthologs U_S3 and $U_S3.5$ (39–41).

Further analysis identified a conserved phosphorylation site within the C termini of both HDAC1 and HDAC2 as the target of ORF66p-mediated phosphorylation. Phosphorylation at this site was responsible for the obvious mobility shift of HDACs present in extracts from VZV-infected cells (Fig. 5). However, in vitro kinase assays suggested that HDAC2 is not a direct substrate for ORF66p kinase activity (Fig. 6). Therefore, ORF66p-dependent phosphorylation of HDAC2 (and most likely HDAC1) occurs through an indirect mechanism. We infer from these results that ORF66p activation of a cellular kinase or pathway leads to hyperphosphorylation of HDAC1 and HDAC2. Previous studies with HSV-1 U_S3 kinase demonstrated that it activated cellular PKA (2), although recent studies suggest that ORF66p does not act in a similar manner (A. Erazo and P. R. Kinchington, unpublished data). Indeed, the conserved targets of ORF66p phosphorylation in both HDAC1 and HDAC2 (S406 and S407, respectively) fit consensus sites for the cellular kinases PKA, PKC (HDAC2 only), and PKG. Studies of phosphorylation of murine HDAC2 indicate that PKA is not one of the primary kinases that target this protein (49). Therefore, future studies will concentrate on dissecting the identity of cellular kinases involved in ORF66p-dependent phosphorylation of HDAC1 and HDAC2.

Disrupting or inactivating ORF66p protein kinase affects VZV growth in a cell-type-dependent manner (11, 42, 43, 46). The functional roles of ORF66p that are necessary to direct efficient replication in these various cell types remain undefined. Because hyperphosphorylation of HDAC1 and HDAC2

does not occur in cells infected with ORF66p kinase-deficient virus, we first asked if downregulation of these proteins by RNA interference would complement some of this mutant virus's growth defects. Recombinant retroviruses expressing short hairpin RNAs targeting either nothing or HDAC1 or HDAC2 were used to transduce MeWo cells and generate stable cell lines. While we were initially able to achieve a high knockdown level (~80% and ~85%, respectively), the knockdowns were unstable and HDAC levels rose with cell passage (data not shown). Therefore, as an alternative we investigated the effect of blocking HDAC1 and HDAC2 activity (using the inhibitor sodium butyrate) on replication and growth of an ORF66p kinase-deficient VZV (Fig. 7). Inhibition of HDAC activity had no effect on the plaquing efficiency of wild-type VZV, whereas the plaquing efficiency of VZV-ORF66KD increased by 1.5-fold. In addition, analysis of plaque size highlighted that inhibition of HDAC activity only marginally increased wild-type virus plaque size (1.2-fold) whereas VZV-ORF66KD plaque size doubled (2.2-fold). Consistent with these data, growth curve analysis demonstrated a fourfold increase in overall titer of infectious centers generated by VZV-ORF66KD when HDAC activity was inhibited, whereas no difference was observed for wild-type virus (Fig. 8A). Thus, inhibition of HDAC activity increases the frequency of successful initiation of infection. Subsequent spread and growth of VZV-ORF66KD suggest that ORF66p kinase activity has a role in inhibiting HDAC activity during viral infection. However, inhibition of deacetylase activity results only in partial complementation of the growth defect associated with ORF66p kinase-deficient VZV, suggesting that its kinase activity is required for additional functions other than inhibition of HDAC activity.

Analyses of growth curves revealed differences in growth kinetics between wild-type and kinase-deficient virus. For wild-type virus, the titer increased approximately 7- to 10-fold at 24 hpi, indicating that the eclipse phase was completed in less than 24 h. However, for ORF66p kinase-deficient virus, the eclipse phase was extended to sometime between 24 and 48 hpi. These data indicate that ORF66p kinase activity is required for efficient initiation of replication and support a hypothesis wherein ORF66p kinase activity functions to combat host silencing. There was no difference in expression or accumulation of the four immediate-early VZV proteins ORFs 4p, 61p, 62p, and 63p during infection with wild-type virus between cells that were mock treated and those that were treated with sodium butyrate. In contrast, accumulation of viral proteins for ORF66p kinase-deficient VZV lagged approximately 24 h behind that for wild-type virus, correlating with the extended eclipse phase of this virus in mock-treated and sodium butyrate-treated cells. While sodium butyrate treatment did not reduce the eclipse phase for VZV-ORF66KD, virus yield increased fourfold at 72 hpi compared to that for virus grown in untreated cells and remained at this level. The expression kinetics, accumulation, and abundance of ORFs 4p, 61p, 62p, and 63p also increased in cells treated with sodium butyrate over those in untreated cells, with the most significant difference being observed for ORF61p. These data support our hypothesis that blocking HDAC activity by ORF66p allows efficient VZV replication.

A question that remains is how HDAC-mediated silencing is blocked by ORF66p-dependent hyperphosphorylation of HDAC1 and HDAC2. Phosphorylation of HDAC1 and HDAC2 regulates their enzymatic activity (13, 38, 49). Initial experiments demonstrate no change in HDAC2 enzymatic activity in VZV-infected cells or cells autonomously expressing ORF66p. However, because only a small fraction of HDAC molecules are hyperphosphorylated, it is plausible that our assay was not sensitive enough to detect small changes in enzyme activity. Also, it is not known if phosphorylation at S406/7 regulates HDAC activity, but its proximity to other sites of phosphorylation suggests that multiple kinases targeting this region all affect its activity. Alternatively, hyperphosphorylation of HDAC1 and HDAC2 may regulate interaction of these proteins with other members of the corepressor complexes that they reside in. This is an intriguing hypothesis, as studies with HSV-1 demonstrated that in addition to phosphorylation of HDAC1 and HDAC2 by U_S3 kinases, HDACs are dislodged from their corepressors LSD1/CoREST/REST in a process that requires ICP0 (17–19, 40). Following these events, a portion of HDAC1, HDAC2, LSD1, CoREST, and REST translocates to the cytoplasm by an unknown mechanism (17, 18). Initial studies of protein-protein interactions between HDAC1, HDAC2, CoREST, and REST in VZV-infected cells or cells autonomously expressing ORF66p demonstrated no change in the composition of these complexes compared to those in uninfected cells (data not shown). However, biochemical fractionation of VZV-infected cells showed a modest increase in cytoplasmic accumulation of HDAC1, HDAC2, and CoREST as infection progressed (M. S. Walters and S. Silverstein, unpublished data). Therefore, a similar sequence of events may occur in cells infected with VZV. We are currently attempting to pursue this line of investigation.

In conclusion, we have identified HDAC1 and HDAC2 as new targets for ORF66p kinase activity. During VZV infection, both HDACs are hyperphosphorylated, and this occurs at a single conserved Ser within the C terminus of each protein. In addition, in vitro analysis demonstrated that ORF66p-dependent phosphorylation is indirect. We further investigated the function of this phosphorylation event and demonstrated that inhibition of HDAC activity partially rescues growth defects associated with an ORF66p kinase-deficient VZV. These data suggest a model whereby the presence of tegument-associated ORF66p initiates hyperphosphorylation of HDAC1 and HDAC2, resulting in inhibition of silencing by host HDAC complexes on viral DNA. We therefore propose that an additional function of ORF66p kinase is to suppress host cell silencing of viral DNA in a fashion similar to how HSV-1 U_S3 kinases function.

ACKNOWLEDGMENTS

We thank Christos Kyratsous, Michelle Staudt, and Daniel Wolf for helpful discussions.

This study was supported by Public Health Service grants AI-024021 (S.S.), NS064022 (P.R.K.), and EY08098 (P.R.K.). The work was also supported by funds from The Eye & Ear Foundation of Pittsburgh and Research to Prevent Blindness, Inc. A.E. was a recipient of an NIH predoctoral T32 training grant, AI060525.

REFERENCES

1. **Arvin, A. M.** 1996. Varicella-zoster virus. Clin. Microbiol. Rev. **9:**361–381.
2. **Benetti, L., and B. Roizman.** 2004. Herpes simplex virus protein kinase US3 activates and functionally overlaps protein kinase A to block apoptosis. Proc. Natl. Acad. Sci. USA **101:**9411–9416.

3. **Besser, J., M. Ikoma, K. Fabel, M. H. Sommer, L. Zerboni, C. Grose, and A. M. Arvin.** 2004. Differential requirement for cell fusion and virion formation in the pathogenesis of varicella-zoster virus infection in skin and T cells. J. Virol. **78:**13293–13305.
4. **Bradford, M. M.** 1976. A rapid and sensitive method for the quantitation of microgram quantities of protein utilizing the principle of protein-dye binding. Anal. Biochem. **72:**248–254.
5. **Carpenter, J. E., E. P. Henderson, and C. Grose.** 2009. Enumeration of an extremely high particle-to-PFU ratio for varicella-zoster virus. J. Virol. **83:** 6917–6921.
6. **Cheung, W. L., S. D. Briggs, and C. D. Allis.** 2000. Acetylation and chromosomal functions. Curr. Opin. Cell Biol. **12:**326–333.
7. **Danaher, R. J., R. J. Jacob, M. R. Steiner, W. R. Allen, J. M. Hill, and C. S. Miller.** 2005. Histone deacetylase inhibitors induce reactivation of herpes simplex virus type 1 in a latency-associated transcript-independent manner in neuronal cells. J. Neurovirol. **11:**306–317.
8. **David, G., M. A. Neptune, and R. A. DePinho.** 2002. SUMO-1 modification of histone deacetylase 1 (HDAC1) modulates its biological activities. J. Biol. Chem. **277:**23658–23663.
9. **Eisfeld, A. J., S. E. Turse, S. A. Jackson, E. C. Lerner, and P. R. Kinchington.** 2006. Phosphorylation of the varicella-zoster virus (VZV) major transcriptional regulatory protein IE62 by the VZV open reading frame 66 protein kinase. J. Virol. **80:**1710–1723.
10. **Eisfeld, A. J., M. B. Yee, A. Erazo, A. Abendroth, and P. R. Kinchington.** 2007. Downregulation of class I major histocompatibility complex surface expression by varicella-zoster virus involves open reading frame 66 protein kinase-dependent and -independent mechanisms. J. Virol. **81:**9034–9049.
11. **Erazo, A., M. B. Yee, N. Osterrieder, and P. R. Kinchington.** 2008. Varicella-zoster virus open reading frame 66 protein kinase is required for efficient viral growth in primary human corneal stromal fibroblast cells. J. Virol. **82:**7653–7665.
12. **Fensterl, V., and G. C. Sen.** 2009. Interferons and viral infections. Biofactors **35:**14–20.
13. **Galasinski, S. C., K. A. Resing, J. A. Goodrich, and N. G. Ahn.** 2002. Phosphatase inhibition leads to histone deacetylases 1 and 2 phosphorylation and disruption of corepressor interactions. J. Biol. Chem. **277:** 19618–19626.
14. **Gregoretti, I. V., Y. M. Lee, and H. V. Goodson.** 2004. Molecular evolution of the histone deacetylase family: functional implications of phylogenetic analysis. J. Mol. Biol. **338:**17–31.
15. **Grozinger, C. M., and S. L. Schreiber.** 2002. Deacetylase enzymes: biological functions and the use of small-molecule inhibitors. Chem. Biol. **9:**3–16.
16. **Grunstein, M.** 1997. Histone acetylation in chromatin structure and transcription. Nature **389:**349–352.
17. **Gu, H., Y. Liang, G. Mandel, and B. Roizman.** 2005. Components of the REST/CoREST/histone deacetylase repressor complex are disrupted, modified, and translocated in HSV-1-infected cells. Proc. Natl. Acad. Sci. USA **102:**7571–7576.
18. **Gu, H., and B. Roizman.** 2009. Engagement of the lysine-specific demethylase/HDAC1/CoREST/REST complex by herpes simplex virus 1. J. Virol. **83:**4376–4385.
19. **Gu, H., and B. Roizman.** 2007. Herpes simplex virus-infected cell protein 0 blocks the silencing of viral DNA by dissociating histone deacetylases from the CoREST-REST complex. Proc. Natl. Acad. Sci. USA **104:**17134–17139.
20. **Gwack, Y., H. Byun, S. Hwang, C. Lim, and J. Choe.** 2001. CREB-binding protein and histone deacetylase regulate the transcriptional activity of Kaposi's sarcoma-associated herpesvirus open reading frame 50. J. Virol. **75:** 1909–1917.
21. **Haberland, M., R. L. Montgomery, and E. N. Olson.** 2009. The many roles of histone deacetylases in development and physiology: implications for disease and therapy. Nat. Rev. Genet. **10:**32–42.
22. **Heineman, T. C., and J. I. Cohen.** 1995. The varicella-zoster virus (VZV) open reading frame 47 (ORF47) protein kinase is dispensable for viral replication and is not required for phosphorylation of ORF63 protein, the VZV homolog of herpes simplex virus ICP22. J. Virol. **69:**7367–7370.
23. **Hobbs, W. E., II, and N. A. DeLuca.** 1999. Perturbation of cell cycle progression and cellular gene expression as a function of herpes simplex virus ICP0. J. Virol. **73:**8245–8255.
24. **Hu, H., and J. I. Cohen.** 2005. Varicella-zoster virus open reading frame 47 (ORF47) protein is critical for virus replication in dendritic cells and for spread to other cells. Virology **337:**304–311.
25. **Kenyon, T. K., E. Homan, J. Storlie, M. Ikoma, and C. Grose.** 2003. Comparison of varicella-zoster virus ORF47 protein kinase and casein kinase II and their substrates. J. Med. Virol. **70**(Suppl. 1)**:**S95–S102.
26. **Kinchington, P. R., K. Fite, A. Seman, and S. E. Turse.** 2001. Virion association of IE62, the varicella-zoster virus (VZV) major transcriptional regulatory protein, requires expression of the VZV open reading frame 66 protein kinase. J. Virol. **75:**9106–9113.
27. **Kinchington, P. R., K. Fite, and S. E. Turse.** 2000. Nuclear accumulation of IE62, the varicella-zoster virus (VZV) major transcriptional regulatory protein, is inhibited by phosphorylation mediated by the VZV open reading frame 66 protein kinase. J. Virol. **74:**2265–2277.
28. **Kinchington, P. R., and S. E. Turse.** 1998. Regulated nuclear localization of the varicella-zoster virus major regulatory protein, IE62. J. Infect. Dis. **178**(Suppl. 1)**:**S16–S21.
29. **Kyratsous, C. A., and S. J. Silverstein.** 2009. Components of nuclear domain 10 bodies regulate varicella-zoster virus replication. J. Virol. **83:**4262–4274.
30. **Laemmli, U. K.** 1970. Cleavage of structural proteins during the assembly of the head of bacteriophage T4. Nature **227:**680–685.
31. **Lungu, O., C. A. Panagiotidis, P. W. Annunziato, A. A. Gershon, and S. J. Silverstein.** 1998. Aberrant intracellular localization of varicella-zoster virus regulatory proteins during latency. Proc. Natl. Acad. Sci. USA **95:**7080–7085.
32. **McGeoch, D. J., and A. J. Davison.** 1986. Alphaherpesviruses possess a gene homologous to the protein kinase gene family of eukaryotes and retroviruses. Nucleic Acids Res. **14:**1765–1777.
33. **Montgomery, R. L., C. A. Davis, M. J. Potthoff, M. Haberland, J. Fielitz, X. Qi, J. A. Hill, J. A. Richardson, and E. N. Olson.** 2007. Histone deacetylases 1 and 2 redundantly regulate cardiac morphogenesis, growth, and contractility. Genes Dev. **21:**1790–1802.
34. **Moriuchi, H., M. Moriuchi, H. A. Smith, S. E. Straus, and J. I. Cohen.** 1992. Varicella-zoster virus open reading frame 61 protein is functionally homologous to herpes simplex virus type 1 ICP0. J. Virol. **66:**7303–7308.
35. **Moriuchi, H., M. Moriuchi, S. E. Straus, and J. I. Cohen.** 1993. Varicella-zoster virus (VZV) open reading frame 61 protein transactivates VZV gene promoters and enhances the infectivity of VZV DNA. J. Virol. **67:**4290–4295.
36. **Munger, J., A. V. Chee, and B. Roizman.** 2001. The U_S3 protein kinase blocks apoptosis induced by the *d*120 mutant of herpes simplex virus 1 at a premitochondrial stage. J. Virol. **75:**5491–5497.
37. **Ogg, P. D., P. J. McDonell, B. J. Ryckman, C. M. Knudson, and R. J. Roller.** 2004. The HSV-1 Us3 protein kinase is sufficient to block apoptosis induced by overexpression of a variety of Bcl-2 family members. Virology **319:**212–224.
38. **Pflum, M. K., J. K. Tong, W. S. Lane, and S. L. Schreiber.** 2001. Histone deacetylase 1 phosphorylation promotes enzymatic activity and complex formation. J. Biol. Chem. **276:**47733–47741.
39. **Poon, A. P., H. Gu, and B. Roizman.** 2006. ICP0 and the US3 protein kinase of herpes simplex virus 1 independently block histone deacetylation to enable gene expression. Proc. Natl. Acad. Sci. USA **103:**9993–9998.
40. **Poon, A. P. W., Y. Liang, and B. Roizman.** 2003. Herpes simplex virus 1 gene expression is accelerated by inhibitors of histone deacetylases in rabbit skin cells infected with a mutant carrying a cDNA copy of the infected-cell protein no. 0. J. Virol. **77:**12671–12678.
41. **Poon, A. P. W., and B. Roizman.** 2007. Mapping of key functions of the herpes simplex virus 1 U_S3 protein kinase: the U_S3 protein can form functional heteromultimeric structures derived from overlapping truncated polypeptides. J. Virol. **81:**1980–1989.
42. **Schaap, A., J. F. Fortin, M. Sommer, L. Zerboni, S. Stamatis, C. C. Ku, G. P. Nolan, and A. M. Arvin.** 2005. T-cell tropism and the role of ORF66 protein in pathogenesis of varicella-zoster virus infection. J. Virol. **79:**12921–12933.
43. **Schaap-Nutt, A., M. Sommer, X. Che, L. Zerboni, and A. M. Arvin.** 2006. ORF66 protein kinase function is required for T-cell tropism of varicella-zoster virus in vivo. J. Virol. **80:**11806–11816.
44. **Schwer, B., and E. Verdin.** 2008. Conserved metabolic regulatory functions of sirtuins. Cell Metab. **7:**104–112.
45. **Smith, R. F., and T. F. Smith.** 1989. Identification of new protein kinase-related genes in three herpesviruses, herpes simplex virus, varicella-zoster virus, and Epstein-Barr virus. J. Virol. **63:**450–455.
46. **Soong, W., J. C. Schultz, A. C. Patera, M. H. Sommer, and J. I. Cohen.** 2000. Infection of human T lymphocytes with varicella-zoster virus: an analysis with viral mutants and clinical isolates. J. Virol. **74:**1864–1870.
47. **Stevenson, D., K. L. Colman, and A. J. Davison.** 1994. Characterization of the putative protein kinases specified by varicella-zoster virus genes 47 and 66. J. Gen. Virol. **75:**317–326.
48. **Tavalai, N., and T. Stamminger.** 2008. New insights into the role of the subnuclear structure ND10 for viral infection. Biochim. Biophys. Acta **1783:** 2207–2221.
49. **Tsai, S. C., and E. Seto.** 2002. Regulation of histone deacetylase 2 by protein kinase CK2. J. Biol. Chem. **277:**31826–31833.
50. **Walters, M. S., C. A. Kyratsous, S. Wan, and S. Silverstein.** 2008. Nuclear import of the varicella-zoster virus latency-associated protein ORF63 in primary neurons requires expression of the lytic protein ORF61 and occurs in a proteasome-dependent manner. J. Virol. **82:**8673–8686.
51. **Wang, L., M. Sommer, J. Rajamani, and A. M. Arvin.** 2009. Regulation of the ORF61 promoter and ORF61 functions in varicella-zoster virus replication and pathogenesis. J. Virol. **83:**7560–7572.
52. **Wolf, D., and S. P. Goff.** 2008. Host restriction factors blocking retroviral replication. Annu. Rev. Genet. **42:**143–163.
53. **Yang, X. J., and E. Seto.** 2003. Collaborative spirit of histone deacetylases in regulating chromatin structure and gene expression. Curr. Opin. Genet. Dev. **13:**143–153.